University of Tartu

Faculty of Science and Technology

Institute of Technology

Karl-Mattias Moor

Architecture development and testing for the engineering model of SUTS satellite communication system

Bachelor's thesis (12 ECTS)

Computer engineering

Supervisors:

Jānis Dalbiņš, M.Sc.Eng

Ivo Müürsepp, PhD

Tartu 2025

Abstract/Resümee

Architecture development and testing for the engineering model of SUTS satellite communication system

This bachelor's thesis presents the development and testing of the communication subsystem for the Strategic Upgrades Test Satellite (SUTS), a 3-unit PQ picosatellite developed by the Estonian Student Satellite Foundation. The primary goal was to design an engineering model of the UHF communication system that meets the constraints of small satellite architecture while maintaining reliability and regulatory compliance. The system, which operates in the 435–438 MHz amateur band using Gaussian Frequency Shift Keying (GFSK) modulation, was designed with a focus on simplicity, efficiency, and space optimization by omitting a dedicated MCU and instead relying on control via the main Command and Data Handling System (CDHS). Key components include the Silicon Labs Si4468 transceiver and the GRF5504 power amplifier. The thesis provides an in-depth analysis of the architecture, link budget, PCB layout, and RF chain design, as well as a comprehensive suite of performance tests including gain, efficiency, thermal tolerance, out-of-band emissions, and receiver sensitivity. The results validate the communication subsystem's performance and inform further development toward a flight-ready model.

CERCS: T120 Systems engineering, computer technology; T170 Electronics; T180 Telecommunication engineering; T320 Space technology

Keywords: PocketQube, CubeSat, Satellite communication, SUTS, UHF

SUTS satelliidi sidesüsteemi insenerimudeli arhitektuuri arendus ja testimine

See bakalaureusetöö käsitleb Strateegiliste Uuenduste Testimise Satelliidi (SUTS) sidesüsteemi arendamist ja testimist. SUTS on kolmeühikuline PQ-pikosatelliit, mille on välja töötanud Eesti Tudengisatelliidi Sihtasutus. Töö peamiseks eesmärgiks oli luua UHF-sidesüsteemi insenerimudel, mis vastaks väikesatelliitide arhitektuurilistele piirangutele, säilitades samas töökindluse ja vastavuse regulatsioonidele. Süsteem töötab 435–438 MHz amatöörsagedusribas, kasutades Gaussi sagedusnihkega modulatsiooni (GFSK), ning see on kavandatud lihtsuse, tõhususe ja ruumi kokkuhoiu põhimõtetest lähtuvalt – eraldi mikrokontrolleri (MCU) asemel toimub juhtimine peamise käsu- ja andmetöötlussüsteemi (CDHS) kaudu. Olulised komponendid on Silicon Labs Si4468 raadiosaatja ja GRF5504 võimendi. Töö sisaldab põhjalikku analüüsi süsteemi arhitektuurist, raadioside eelarvest, trükkplaadi ja raadiosagedusahela disainist, samuti ulatuslikku testide komplekti, mille hulka kuuluvad võimenduse, tõhususe, termilise taluvuse, sagedusväliste kiirguste ja vastuvõtutundlikkuse mõõtmised. Tulemused kinnitavad sidesüsteemi töökindlust ja pakuvad sisendit edasiseks arenduseks lennuvalmis mudeli suunas.

CERCS: T120 Süsteemitehnoloogia, arvutitehnoloogia; T170 Elektroonika; T180 Telekommunikatsioonitehnoloogia; T320 Kosmosetehnoloogia

Võtmesõnad: PocketQube, CubeSat, Satelliitside, SUTS, UHF

Contents

List of Figures

List of Tables

Acronyms

ADC Analog-to-Digital Converter. 29

ADCS Attitude determination and control system. 14

CDHS Command and Data Handling System. 17, 23, 41

COM Communication system. 6, 16, 17, 23, 29, 37, 39

dB Decibel. 20, 22–24, 27, 28, 31, 33, 35, 40, 41

dBi Decibels relative to an isotropic radiator. 19

dBm Decibel-milliwatts. 17–19, 21–23, 25, 32, 33, 39, 41

DUT Device under test. 38

FM Frequency Modulation. 14

FSPL Free-space path loss. 19

GFSK Gaussian frequency-shift keying. 14, 18, 22–24, 35, 36

GMSK Gaussian minimum shift keying. 14

IEEE Institute of Electrical and Electronics Engineers. 11

IoT Internet of Things. 14

LDMOS Laterally diffused metal–oxide–semiconductor. 13

LNA Low Noise Amplifier. 27, 28

MCU Microcontroller unit. 13, 14, 23, 41

MHz Megahertz. 24, 33

OOK On-Off Keying. 14

PA Power amplifier. 6, 25–27, 29, 31, 32, 34, 38, 41

PAE Power-Added Efficiency. 24, 32, 41

PCB Printed circuit board. 29

PQ PocketQube. 11, 13, 14, 16

RF Radio frequency. 13, 17, 24, 29, 31, 32, 37, 41

RSSI Received Signal Strength Indicator. 39–41

SUTS Strategic Upgrades Test Satellite. 6, 11, 12, 16, 17, 19, 23, 24, 29

TLE Two-line element. 19

UHF Ultra high frequency. 14

VNA Vector network analyzer. 32

1 Introduction

Access to space has become cheaper and more accessible over the last decades, mainly due to the standardization of spacecraft such as CubeSat and PocketQube (PQ) standards [1]. CubeSats are small satellites made of 10x10x10 cm units that can weigh up to 2 kg per cube [2]. In 2018, the PQ standard was established. This standard proposes an even smaller form factor of 5x5x5 cm, which further reduces the cost and helps universities build satellites for educational purposes [3].

The most common way satellites communicate with Earth is through a radio frequency signal in the range of 30 MHz – 60 GHz. The Institute of Electrical and Electronics Engineers (IEEE) divides this frequency range into letter-designated frequency bands [4]. The communications link consists of a radio transmitter, a free-space communication channel, and a radio receiver. In the case of satellite communication, both the satellite and the operator on the ground require a transmitter and a receiver for two-way communication. If the satellite is transmitting, the communication is called downlink, but if the ground station is transmitting, the communication is called uplink. In the case of satellites, both a receiver and a transmitter are required, which in many cases are combined into a transceiver. Typically, a communication system of a small satellite mission consists of a transceiver comprised of a radio, a power amplifier, and an antenna. [5]

This bachelor's thesis focuses on the development and testing of the communication system for the Strategic Upgrades Test Satellite (SUTS). SUTS is a 3-unit PQ developed by the Estonian Student Satellite Foundation. The development of SUTS began in 2023 and the satellite is expected to launch in 2028. The main mission of SUTS is to test two payloads provided by industry and academic partners: an optical communications module developed by Estonian companies Golbriak Space and Skudo, and a lunar regolith solar cell test area developed by Tallinn University of Technology. The planned orbit of SUTS is a 550 km Sun-synchronous low Earth orbit. The satellite platform includes the aluminum structure, the Command and Data Handling System, the Electrical Power System, the UHF Communication System, and the

Attitude Determination and Control System. The platform is entirely designed by the Estonian Student Satellite Foundation.

The thesis provides an overview of the communication system architecture for SUTS and describes the development and testing of the engineering model. This thesis gives an overview of the communication systems of similar missions in chapter 2, and describes the work done in this thesis in chapter 3 and chapter 4.

2 Similar missions

The following chapter provides a brief overview of the Estonian CubeSat mission ESTCube-2 and the PQ missions MRC-100 and Delfi-PQ, and their communication system hardware architecture.

2.1 ESTCube-2

ESTCube-2 was a three-unit CubeSat developed by the Estonian Student Satellite Foundation. The main goal of ESTCube-2 was to demonstrate the electric solar wind sail (E-sail) in the ionosphere of Earth, where it can be used as an ionospheric plasma brake for deorbiting. As secondary payloads, the satellite had two cameras on board to measure the normalized difference vegetation index, and a corrosion testing experiment was conducted to test the corrosion behavior of different coating materials. ESTCube-2 launched on 9 October 2023, on board the Vega rocket from Kourou, French Guiana, but failed to deploy from the rocket. [6, 7]

The communication system of ESTCube-2 consists of two hot redundant subsystems: primary communications (PCOM) and a backup subsystem called secondary communications (SCOM). PCOM can transmit and receive on the 70 cm radio amateur band, and SCOM can receive on the 2 m band and transmit on the 70 cm band. The processing unit of PCOM is an STM32L4 series microcontroller from STMicroelectronics, and Radio Frequency (RF) connectivity is achieved by the Silicon Labs Si4463 transceiver. An NXP high-robustness wide-band RF power Laterally Diffused Metal–Oxide–Semiconductor (LDMOS) transistor amplified the transmission signal. SCOM uses a Silicon Labs EZR32WG330 series Microcontroller Unit (MCU) with a built-in RF transceiver module. For transmission, the subsystem can change its carrier frequency to the 70 cm band and use PCOM's RF path to transmit the signal as a backup transmitter. [8, 9]

2.2 MRC-100

MRC-100 is a 3-P PQ class student satellite developed by the Budapest University of Technology and Economics. It is a continuation of previous Hungarian satellites: SMOG-P, ATL-1, and SMOG-1. The main goals of the mission were to test multiple RF payloads developed in-house, including a spectrum analyzer (30 – 2600 MHz), 1 Mbit/s S-band downlink, an automatic identification system receiver, and a Ultra High Frequency (UHF)-band LoRa-GPS Tracker. MRC-100 was launched on June 12th, 2023 on board a Falcon 9 rocket. [10]

The communication system of the MRC-100 is based on the Acsip S62F LoRa and FSK radio module type S62F with an external MCU. The antenna is a V-shaped 2x quarter-wavelength dipole. Due to subsystem-level redundancy, two independent telecommand receivers and two telemetry transmitters were connected to the antenna, creating a cold redundant, half-duplex system. The telemetry and telecommand system uses On-Off Keying (OOK), 2-Gaussian Minimum Shift Keying (GMSK) and LoRa-type linear Frequency Modulation (FM) chirp. The internationally coordinated operation bandwidth of the communication system of MRC-100 is 12.5 kHz for uplink and 20 kHz for downlink [11].

2.3 Delfi-PQ

Delfi-PQ is a 3-P PQ class student satellite developed by the University of Delft. The mission's main goals were to provide students with practical experience in the space engineering field, to develop a baseline PQ platform for future missions, and to test several payloads from the University of Delft that need in-orbit validation. The long-term overall goal is to develop 3P PQ and to manage, through miniaturization, to fit the core bus in 1P, micropropulsion, and Attitude Determination and Control System (ADCS) in the second 1P, and an innovative payload within the remaining 1P. Delfi-PQ was launched on January 13th, 2022, on board a Falcon 9 rocket and was operational until January 1st, 2024. [12, 13]

The communication system of the Delfi-PQ is based on the Semtech SX1278, a LoRa transceiver intended for Internet of Things (IoT) applications. The transceiver features a Gaussian Frequency-Shift Keying (GFSK)/GMSK radio engine and a separate LoRa one. AX.25 support has been implemented to allow radio amateurs to receive telemetry, and a custom protocol was also implemented to experiment with advanced forward error correction schemes. A high-power high-efficiency power amplifier has also been designed, allowing a maximum 1 W output power with an efficiency greater than 64%. Additionally, a low-power mode (250

mW) was implemented with an efficiency greater than 60%. The antenna system consists of monopole antennas connected to the satellite using rotating elbows and springs. The system uses the 140 – 170 MHz frequency range in the VHF band for uplink and the 390 – 450 MHz frequency range in the UHF band for downlink. [14]

2.4 Takeaways from similar missions

The missions discussed in this chapter: ESTCube-2, MRC-100, and Delfi-PQ, show different approaches to developing communication systems for small satellites. Each project has its own requirements and design priorities which affect the design and development of the system. Despite their differences, they share several common features, such as reliance on COTS components and operation within amateur radio bands. These examples are useful reference points for the SUTS mission in terms of system architecture, component selection, and the trade-offs involved in balancing complexity, reliability, and available resources.

3 Design of the communication system engineering model

The main functionality of the SUTS Communication System (COM) system is to provide a data link between the ground station and the satellite's Command and Data Handling System. SUTS COM is a half-duplex system that uses a time division duplexing scheme. The system will use the 70 cm radio amateur frequency band. Two prototypes of the SUTS COM system were previously developed by Ergo Haavasalu as part of his bachelor's thesis [15]. This thesis aims to continue the previous work and design and verify the engineering model of the SUTS COM system. The main design aspect of the SUTS mission is that everything must fit in the PQ satellite form factor. This imposes constraints on the redundancy and complexity of the system. This chapter describes the design of the SUTS COM system.

3.1 Communication system requirements

Firstly, requirements for the COM system had to be defined based on the overall mission and system requirements, and regulatory standards. The defined requirements can be seen in 3.1.

Table 3.1. Communication system requirements

ID	Requirement	Rationale	Verification
REQ-COM-01	COM shall provide uplink and downlink between the satellite and the ground station.	Both the up- and downlink between the satellite and the ground station are needed for successful satellite operations.	Testing
REQ-COM-02	COM shall be able to transmit with at least 9600 bits per second.	A minimum data rate of 9600 bps ensures that the satellite can efficiently transmit telemetry, payload data, and operational status updates within the available communication windows.	Review of design, testing
REQ-COM-03	COM shall operate without a dedicated microcontroller and be controlled directly by the Command and Data Handling System (CDHS)	Omitting a separate microcontroller reduces system complexity and conserves space within the satellite's limited form factor.	Review of design
REQ-COM-04	COM shall communicate through RF link with 435 - 438 MHz frequency range.	This is the planned frequency range for SUTS in the 70 cm amateur radio frequency band.	Review of design, testing
REQ-COM-05	COM shall have a transmit power of at least 30 dBm.	A minimum transmit power of 30 dBm ensures a strong signal that can reach the ground station reliably, overcoming potential interference and path loss.	Review of design, testing

REQ-COM-07	COM shall use GFSK as the modulation scheme.	GFSK offers narrower bandwidth and improved spectral efficiency, making it well-suited for low-power systems. However, it introduces inter-symbol interference (ISI), which increases receiver complexity.	Review of design
REQ-COM-08	COM shall have a receiver sensitivity of at least -100 dBm.	A receiver sensitivity of at least -100 dBm ensures the communication system can reliably receive weak signals from the ground station	Review of design, testing
REQ-COM-09	COM shall comply with ITU regulations [16] for satellite communication.	Ensures legal operation and prevents interference with other services in the allocated spectrum.	testing, Compliance review
REQ-COM-10	COM should support adaptive power control based on link quality.	Dynamically adjusting the transmit power based on signal strength helps optimize power consumption and improve link reliability.	Testing

3.1.1 Link budget

Since SUTS uses COM only to send commands on the uplink and receive telemetry on the downlink, high data rates are not needed. Dependent on REQ-COM-02, a data rate of 9600 bps was chosen. Based on preliminary simulations using a Two-Line Element (TLE) that matches the proposed orbit of SUTS, there should be approximately seven communication windows per day. The passes were simulated in the Orbitron open source satellite tracking system [17], with an average communication window length of eight minutes, where the satellite is above 5 degrees of elevation. This gives a total data budget of around 32 MB per day. The link budget is split into two separate budgets: one for the uplink and another for downlink. The ground stations in the TUT Mektory building in Tallinn, the University of Tartu Physicum building in Tartu, and the Tartu Observatory in Tõravere will be used for mission operations, but the link budget is calculated for the ground station in Tõravere on the roof of the Tartu Observatory ($58.2654509°\mathrm{N},\ 26.4651677°\mathrm{E}$). For the link budget calculation, the transmit power of the ground station, ground station antenna gain and pointing loss, free space path loss, satellite receiver antenna gain, polarization loss, and losses in the satellite receiver are considered. The transmit power of the ground station is expected to be 47 dBm, and the antenna gain is 23 dBi for the UHF Yagi antenna. The transmit power of the satellite is 30 dBm and the satellite antenna is a monopole with an imperfect ground plane. An antenna prototype was developed by Katarina Aas and a gain of 2 dBi was measured [18]. The largest contributor to attenuation in a satellite link is Free-Space Path Loss (FSPL). It is the attenuation of energy as it spreads spherically into space from the transmitter's antenna. The formula for FSPL can be derived from the Friis transmission formula:

$$\frac{P_r}{P_t} = G_t G_r \left(\frac{\lambda}{4\pi r}\right)^2. \tag{3.1}$$

Where P_r is the power received by the receiving antenna, P_t is the transmitted power, G_t is the gain of the transmitting antenna, G_r is the gain of the receiver antenna, λ is the wavelength of the signal used and r is the distance between the antennas. This equation gives the relationship between the received and transmitted power, where the remaining term is FSPL. The free space path loss is given as 3.2 [19]

$$L_F = \left(\frac{4\pi r f}{c}\right)^2 \tag{3.2}$$

Where f is the frequency of the used signal, r is the distance between the antennas and c is the speed of light in vacuum. When expressed in decibels, with frequency f in megahertz and

distance r in kilometres, we obtain where the last term needs to be multiplied by 10^9 to account for the change in units in the previous terms.

$$L_{F(dB)} = 20\log_{10}(r_{km}) + 20\log_{10}(f_{MHz}) + 20\log_{10}\left(\frac{4\pi \cdot 10^9}{c}\right) \tag{3.3}$$

The lowest angle of elevation of the satellite considered for communication is $5°$. Below this angle, there might be interference from objects such as trees or hills. The distance to the satellite or slant range can be found with the following formula:

$$r = \sqrt{R^2 + (R+H)^2 - 2R(R+H)\sin\left[\varepsilon + \sin^{-1}\left(\frac{R}{R+H}\cos\varepsilon\right)\right]} \tag{3.4}$$

Where *R* is the radius of the Earth, H is the altitude of the satellite, and ε is the elevation angle [20]. A visualization of this can be seen in Figure 3.1.

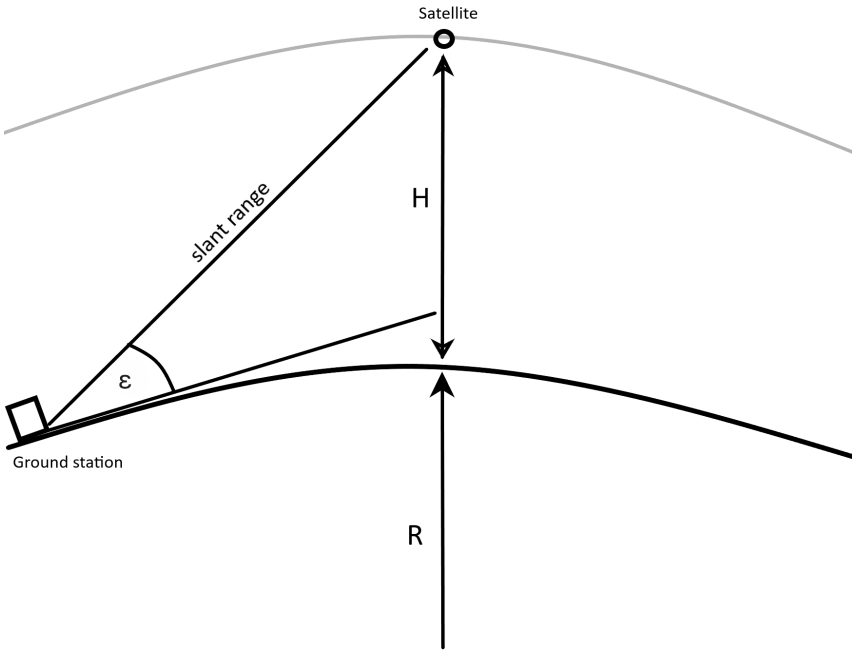

Figure 3.1. Slant range

At 5 degrees, the distance from the satellite is around 2200 km. Based on this,

$$L_{F(\text{db})} = 20\log_{10}(2200) + 20\log_{10}(437) + 32.4 = 152.1\,\text{dB}. \tag{3.5}$$

The crossed Yagi antenna of the ground station is circularly polarized, and the antenna on the satellite is linearly polarized. The reception of the circularly polarized signal with a linearly polarized antenna introduces polarization loss of 3 Decibel (dB) [21]. The receiver's noise floor, estimated losses in the receiver and the E_b/N_0 requirement for the bit-error rate are included

in estimating the theoretical sensitivity. The receiver noise power can be calculated with the following equation.

$$P_{n(\text{dBm})} = 10\log_{10}\left(kT_{sys}B\right) + 30 \tag{3.6}$$

Where k is the Boltzmann constant ($1.38 \cdot 10^{-23}$ J/K), T_{sys} is the system noise temperature, and B is the bandwidth. 30 is added to get the result in dBm. The system noise temperature is not simply a direct sum of noise contributions; rather, it is a weighted combination that accounts for losses and efficiencies along the signal path. As shown in equation 3.7, each noise component is scaled according to the corresponding radiation or chain efficiency. [22]

$$T_{\text{sys}} = \underbrace{T_A}_{\substack{\text{antenna}\\ \text{external}}} + \underbrace{T_P\left(\frac{1}{e_A} - 1\right)}_{\substack{T_{AP},\\ \text{antenna internal}}} + \underbrace{\frac{1}{e_A}T_{RC}\left(\frac{1}{e_L} - 1\right)}_{\text{TL internal}} + \underbrace{\frac{1}{e_A e_L}T_R}_{\text{receiver}}, \tag{3.7}$$

Where T_{sys} is the noise temperature of the system, T_A is the antenna temperature, e_A is the antenna radiation efficiency, T_{RC} is the reception chain temperature e_L is the reception chain efficiency and T_r is the receiver noise temperature.

The external antenna noise temperature is the weighted average of the physical temperatures of all objects and backgrounds within the antenna's field of view, where the weights are determined by the antenna's radiation pattern and the angular distribution of the thermal radiation. As the antenna has an omnidirectional radiation pattern, it can be assumed that half of the antenna is pointed toward Earth with an average temperature of 300 K and half is pointed to space, where noise at 437 MHz due to galactic radiation is around 250 K [22]. The estimated worst-case scenario for the physical temperature of the antenna is 380 K and the antenna efficiency is estimated to be around 90% based on prototype measurements. The loss in the reception chain was calculated to be around 3 dB by adding together the attenuation of all components given in their datasheets and the estimated highest possible physical temperature of the reception chain is 320 K [23] [24]. From this, the efficiency is calculated.

$$e_L = \frac{1}{10^{3/10}} = 0.5 \tag{3.8}$$

The receiver noise temperature was calculated by first finding the noise figure from 3.9 [25]

$$\text{Sensitivity}_{\text{dBm}} = 10 \cdot \log(kTB) + 30 + NF + SNR. \tag{3.9}$$

Sensitivity and the corresponding frequency and bandwidth were taken from the datasheet of the transceiver [26]. Signal to noise ratio(SNR) consists of two terms: the E_b/N_0 corresponding

to the desired bit-error rate and bitrate divided by the bandwidth. When replacing the values and solving for NF we get

$$\text{NF} = -110 - 10 \cdot \log(k \cdot 320 \cdot 40000) - 30 - (12 + 10\log(\frac{40000}{40000}) = 5.53 \tag{3.10}$$

Then noise temperature can be calculated

$$T_n = (10^{\frac{NF}{10}} - 1) \cdot 320 = 823.27K \tag{3.11}$$

Now by putting the calculated values into equation 3.7 we get.

$$T_{\text{sys}} = \underbrace{275}_{\substack{\text{antenna} \\ \text{external}}} + \underbrace{380\left(\frac{1}{0.9} - 1\right)}_{\substack{T_{AP}, \\ \text{antenna internal}}} + \underbrace{\frac{1}{0.9} \cdot 320\left(\frac{1}{0.5} - 1\right)}_{\text{TL internal}} + \underbrace{\frac{1}{0.5 \cdot 0.9} \cdot 823}_{\text{receiver}} = 2501.7K \tag{3.12}$$

Using equation 3.6 we can now calculate the receiver noise power.

$$P_n = 10\log_{10}(k \cdot 2501.7 \cdot 20000) + 30 = -121.6\,\text{dB} \tag{3.13}$$

Table 3.2. Uplink link budget

Uplink link budget, 9600 GFSK		
Ground station transmit power	47	dBm
Ground station antenna gain	23	dBi
Free space path loss	-152.1	dB
Satellite antenna gain	2	dBi
Polarization loss	3	dB
Total power at satellite receiver	-87.1	dBm
Receiver noise power	-121.6	dBm
E_b/N_0 requirement	12	dB
Theoretical sensitivity	-109.6	dBm
Theoretical link margin	22.5	dB

Table 3.3. Downlink link budget

Downlink link budget, 9600 GFSK		
Satellite transmit power	30	dBm
Satellite antenna gain	2	dBi
Free space path loss	-152.1	dB
Ground station antenna gain	23	dBi
Polarization loss	3	dB
Total power at ground station receiver	-100.1	dB
Receiver noise power	-133.8	dBm
Estimated receiver noise figure	3	dB
E_b/N_0 requirement	12	dB
Theoretical sensitivity	-118.8	dBm
Theoretical link margin	18.7	dB

3.2 SUTS Communication system architecture

The top-level diagram of the SUTS COM system can be seen in Figure 3.2. The system consists of the transceiver, the UHF RF front-end, and the analog measurement functional block. The main difference from other nano- and picosat communication systems is that SUTS COM does not have a separate MCU. It is controlled by the CDHS MCU. This was chosen to simplify the overall architecture of the satellite and save space. The transceiver shall communicate with CDHS via SPI.

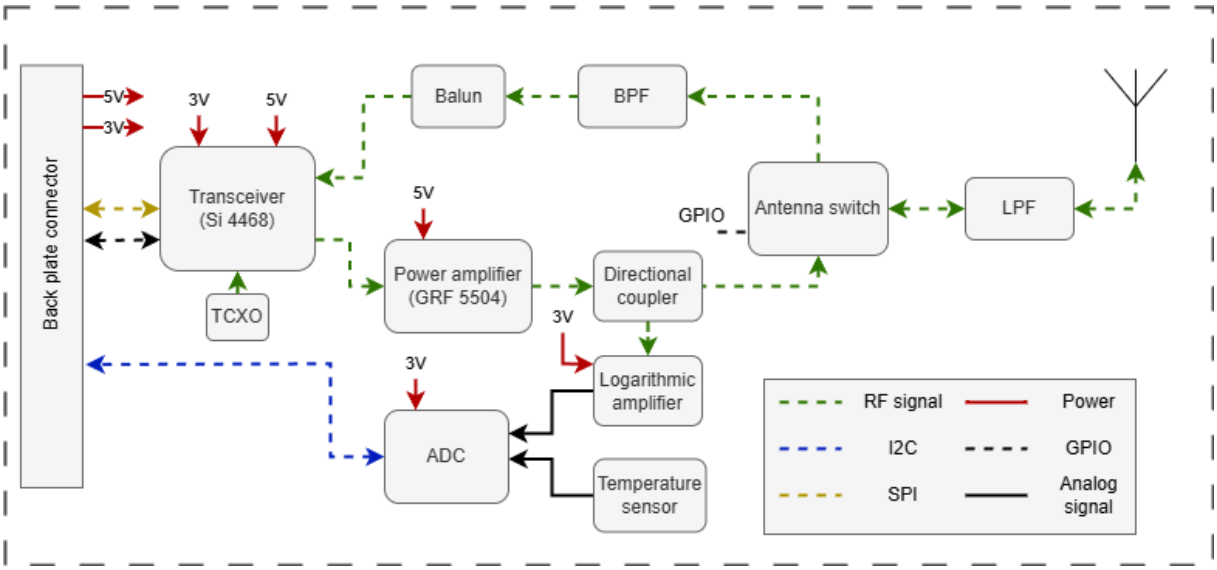

Figure 3.2. Block diagram of SUTS COM system

3.2.1 Transceiver

For SUTS , the Silicon Labs Si4468 transceiver was chosen. A related model, the Si4463, was previously used on the ESTCube-2 satellite, providing valuable experience with the Si446x platform. This transceiver was chosen due to its compliance with requirements and previous experience with the platform. Si4468 is a low-current transceiver with a frequency range of 142-1050 MHz. It supports (G)FSK, (G)4FSK, (G)MSK, and on-off keying as modulation schemes [26]. GFSK was chosen as it reduces power in the sideband due to smoother transitions between frequencies [27]. These parameters comply with REQ-COM-04 and REQ-COM-07.

3.2.2 Power amplifier

Based on the work of Haavasalu, the GRF5504 by Guerrilla RF was chosen. Haavasalu's thesis presented a comprehensive comparison of power amplifiers, and the GRF5504 was chosen and tested. The test results matched the parameters given in the datasheet, and the power amplifier was considered suitable for the application [15]. The amplifier has a wide range of input voltage from 2.7 - 5.5 V, a gain of up to 40 dB, and Power-Added Efficiency (PAE) of up to 61% [28]. This complies with REQ-COM-05. Additionally, Guerrilla RF provides predefined matching networks for 435 MHz, designed to ensure proper impedance matching to 50Ω. Since 437 Megahertz (MHz) is sufficiently close in frequency, these same matching network designs can be used without modification.

3.2.3 Radio frequency chain

The RF chain consists of the transmit and receive chains, which are connected to the antenna through the RFSW1012 antenna switch. The transmission chain includes the GRF5504 power amplifier and the BDCN-20-13+ directional coupler to measure transmission power. The receive chain includes the balun and SF2446E band-pass filter. In addition, there is the LFCN-490D low-pass filter at the antenna switch output. In the transmit chain, impedance matching is required between the transceiver's output and the power amplifier's input. In the application note AN648 of the transceiver, its load impedance is given as

$$Z_{Load} = \left(\frac{0.2815}{\omega_0 \cdot C_s}\right) e^{j \cdot 49.0524^\circ}, \tag{3.14}$$

where ω_0 is angular frequency that corresponds to the operating frequency and C_s is given in the application note as 2.5 pF [29].

$$Z_{Load} = \left(\frac{0.2815}{2\pi \cdot 4.37 \cdot 10^8 \cdot 2.5 \cdot 10^{-8}} \right) e^{j \cdot 49.0524^\circ} = 27 + \text{j}31\ \Omega. \tag{3.15}$$

At an operating frequency of 437 MHz, this gives a load impedance of 27 + j31 Ω. The output impedance of the transceiver is the complex conjugate of the load impedance, which is $27 - j31\Omega$. The impedance of the input port of the power amplifier itself is not explicitly specified, but the custom tuning application note provides a two-element matching network to 50 Ω for 435 MHz, which is sufficiently close to the system's operating frequency to be applicable [30].

There is also a parallel RL chain for biasing and a series-resonant LC tank for harmonic termination. The values of the components were chosen according to the instructions in the transceiver application note [29]. The pull-up inductor value L_{choke} was chosen first. The application note provides different inductance values for various operating frequencies; the closest to the system's frequency is 460 MHz, for which a 220 nH inductor is recommended. Secondly, values for the $L_0 - C_0$ series resonant tank were chosen. A value of 8.2 pF is suggested for C_0. Then, the value of L_0 can be calculated with 3.16 so that it resonates with C_0 at the operating frequency.

$$L_0 = \frac{1}{4\pi^2 f_0^2 C} \approx 16\ \text{nH}. \tag{3.16}$$

Next, the value for the voltage limiting resistor R_{DC} was calculated. In the datasheet of the power amplifier, it is shown that the amplifier is most efficient at 35 dBm output power. To this output power corresponds the input power of -4 dBm or 0.4 mW. As the output power of the transceiver can be reduced in software but not increased, to have a safety margin, a value of 0 dBm or 1 mW was chosen. The output power P_{out} is related to R_{DC} with the following equations.

$$V_{DD\_PA} = \sqrt{\frac{P_{out}}{\pi \omega_0 C_{shunt}}} \approx 0.22\ \text{V}, \tag{3.17}$$

$$I_{DD\_PA} = \pi \omega_0 C_{shunt} V_{DD\_PA} \approx 4.7\ \text{mA}, \tag{3.18}$$

$$R_{DC} = \frac{V_{DD} - V_{DD\_PA}}{I_{DD\_PA}} = 655\ \Omega. \tag{3.19}$$

The closest resistor value available is 680 Ω.

The required values of the matching components are calculated to transform the input impedance of the Power Amplifier (PA) (50Ω) to the desired load impedance of (27 + j31 Ω). The matching circuit was created in the uSimmics circuit simulation software [31]. Where 27 - j31 Ω was

used as the output impedance of the transceiver, and this was matched to 50 Ω. This was done using an L-shaped matching network consisting of two inductors. Using the tuning tool and a Smith chart in Usimmics, values for the inductors were determined. The matching network can be seen in Figure 3.3. To minimize reflections, one needs to get S11 and S22 as low as possible and in the Smith chart they should be as close as possible to the middle 50 Ω point. The goal of this network is to match the output impedance of the transceiver to the input of the power amplifier. As the input impedance of the power amplifier is 50 Ω, getting an output impedance of 50Ω is the best possible outcome. An inductance value of 2 nH for the series inductor and an inductance value of 21 nH gave the best result. The series matching inductor was combined with L_0 for a total value of 19 nH, as this is not a standard value, 18 nH was used.

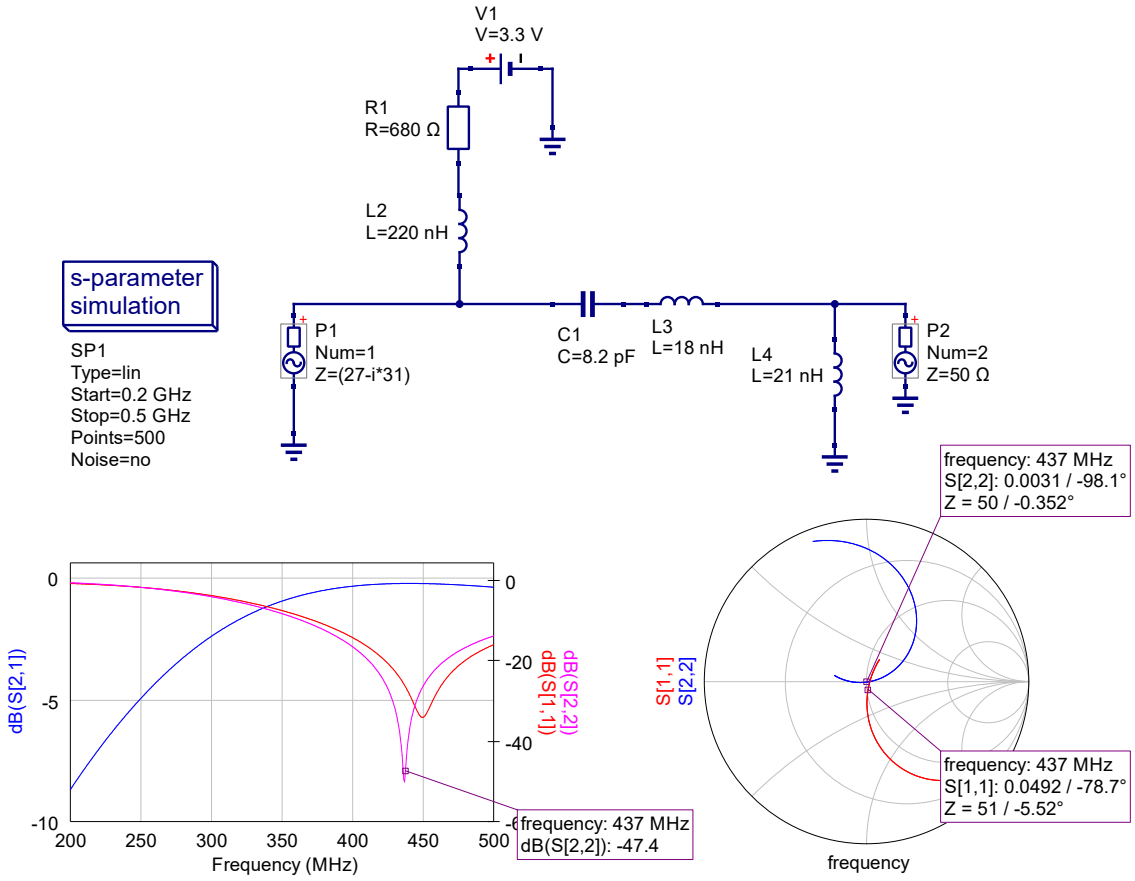

Figure 3.3. Usimmics simulation of PA matching network. In the upper part of the figure, the matching circuit can be seen. Below are graphs that show the S11, S21, and S22 scattering parameters. Matching is good at 437 MHz.

In the application note, a different topology is suggested for matching, consisting of a series inductor and a parallel capacitor. The suggested values for this matching network are given for 460 MHz. The given values are $L_0 = 30nH, C_0 = 8.2pF, C_m = 13pF$. Simulating this in Usimmics gives a very poor match, as can be seen in Figure 3.4. This might imply that

there is a mistake in the load impedance or the matching network given in the application note. The mistake could also have occurred in setting up the simulation. This shall be verified with measurements on the assembled prototype.

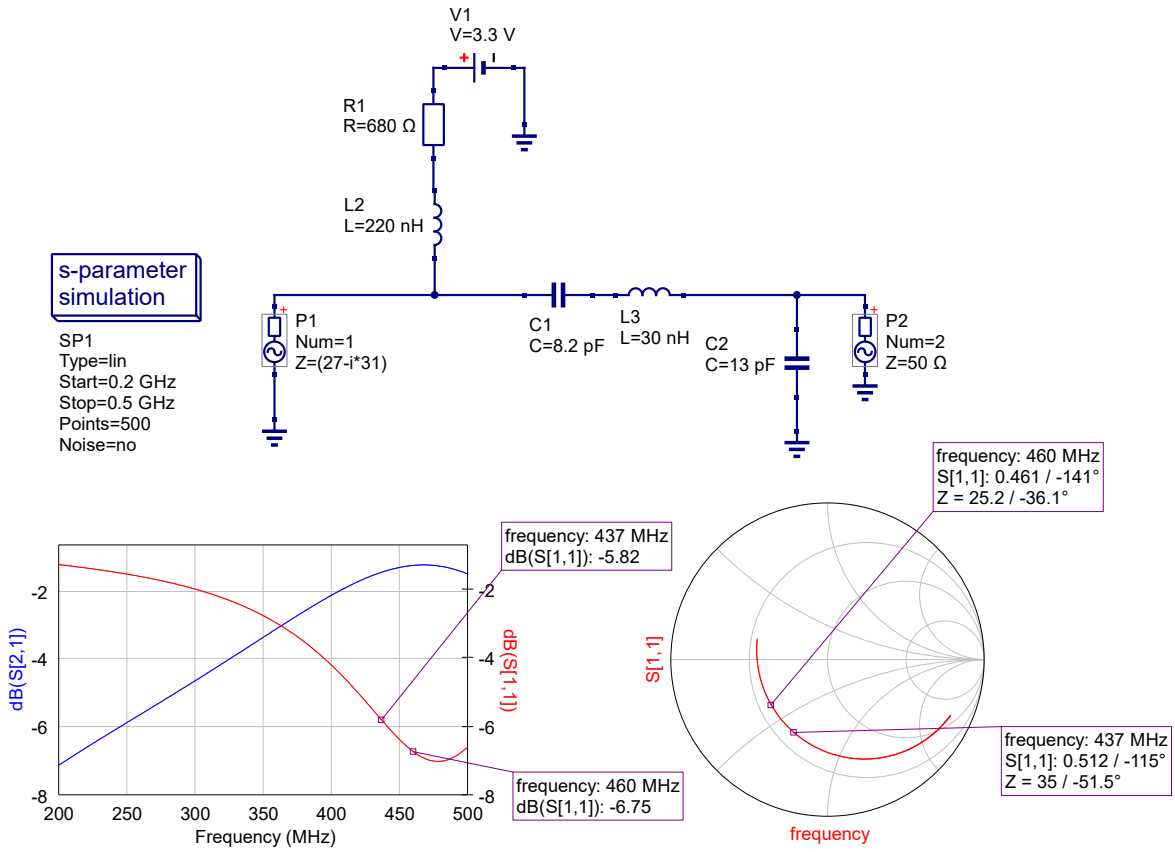

Figure 3.4. Usimmics simulation of PA matching network suggested in the application note. Matching is bad.

After the power amplifier, the transmission chain continues with the BDCN-20-13+ directional coupler [32]. The coupler is used to measure transmit power. This component was chosen because it has a low mainline loss at 437 MHz of only 0.15 dB and can handle up to 15 W of power. The coupled ports of the device are connected to logarithmic amplifiers. All ports of the coupler are matched to 50 Ω. The measuring system is described in more depth in the 3.2.4 sub-chapter.

The receive chain consists of the balun and SF2446E band-pass filter. Matching of the RX side of the transceiver is described in the application note AN643: Si446x/Si4362 RX Low Noise Amplifier (LNA) Matching [33]. The purposes of the matching network are to match the input of the internal LNA to the source impedance as well as to provide a single-ended-to-differential conversion, i.e., a balun, as the LNA is a differential amplifier requiring two input signals. In the application note, three-element and four-element matching networks are

provided. The four-element matching network was chosen as it provides a theoretically perfect phase balance $180°$ between the input pins of the differential amplifier. The input impedance of the LNA has been measured by Silicon Labs at various frequencies, including 434 MHz, where the impedance was 182.65 - j233.09 Ω. The values of the matching network are given in the datasheet. For verification, this was simulated in Usimmics. In the simulation, the input impedance was replaced with an equivalent parallel RC circuit (R1-C3), the values of which were given in the datasheet. Additional ports were added for measuring the phase difference as there is no way to measure in Usimmics without adding ports to the necessary places. The port impedance was set to 1 MΩ so that it would not affect the impedance measurement. The ports are used only for the phase measurements and not for simulating the input impedance. The simulation in Figure 3.5 shows a good match and a phase difference of $183°$ that is close to ideal.

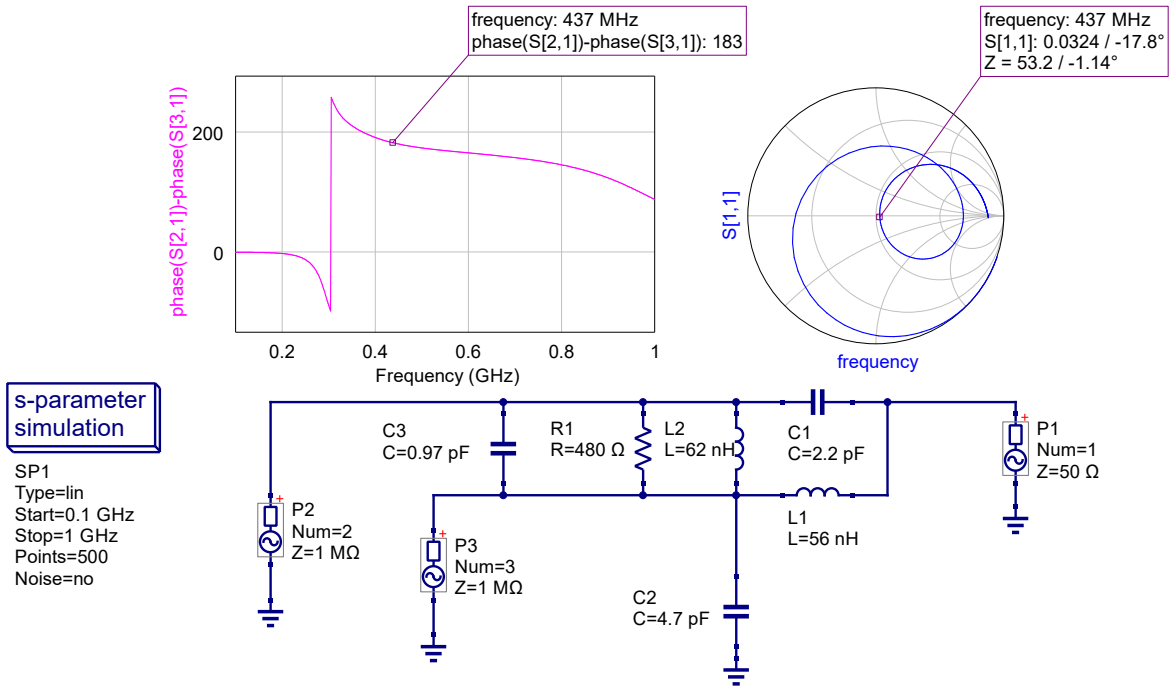

Figure 3.5. Usimmics simulation of balun and RX matching network in the application note. Matching is good at 437 MHz and differential ports are 183 degrees out of phase.

The other part of the reception chain is the SF2446E SAW filter, which filters out emissions at other frequencies[23]. In the frequency range of 430 to 440 MHz, the filter has an average insertion loss of only 1.9 dB, which is lower than most other available options. Both ports of

the filter have an impedance of 50 Ω.

3.2.4 Sensors and power measuring

The measuring system consists of the AD7991 Analog-to-Digital Converter (ADC), two AD8310 logarithmic amplifiers from Analog Devices [34][35]. The inputs of the logarithmic amplifiers are connected to the coupled ports of the directional coupler. In addition, there is an LM26LV temperature sensor by Texas Instruments connected to the ADC near the PA [36]. The goal of the measuring setup is to monitor the temperature and reflected power of the transmit chain to prevent power amplifier failure due to mismatch or high temperatures.

3.3 COM system printed circuit board layout

In (RF) systems, the design of Printed Circuit Board (PCB) plays a pivotal role in ensuring the performance, reliability, and efficiency of the overall COM system. An optimized PCB layout minimizes signal loss, improves power distribution, and reduces the risk of interference, all of which are crucial to maintaining signal integrity. The key factors in the design of the RF system PCB include strategic placement of components, signal routing, and careful design of grounding and shielding. These considerations help mitigate the effects of noise and crosstalk, improving the overall bandwidth and functionality of the system [37].

The compact form factor of the SUTS satellite restricts the size of PCBs to 48 by 46 mm. The small size of PCB imposes even further constraints on the layout. For this reason, a 4-layer impedance-controlled stackup (JLC04161H-2116D) from JLCPCB was chosen. A detailed description of the stackup can be found in the Appendix A. The top layer and the first internal layer form a coplanar waveguide. The trace widths for the RF signals were optimized using the Saturn PCB Toolkit coplanar waveguide calculator, ensuring precise impedance matching to the 50 Ω requirement for the transmission and reception chains [38].

4 Communication system testing

Since the launch of the first satellites, the engineering philosophy has been dominated by highly reliable and thoroughly tested designs. With the rise of the popularity of CubeSats, this has changed in favor of using state-of-the-art and commercial-off-the-shelf components to reduce development time and cost. These improvements come with the cost of reduced reliability as the components and satellites are less tested. A survey of 178 CubeSats conducted in 2014 showed that CubeSats had much lower reliability than other satellites. In the breakdown of failures caused by the subsystem, the communication subsystem is responsible for almost 30% of all failures. In the event of a communication system failure, the mission is compromised due to the inability to maintain communication. In contrast, failure of other systems, such as attitude determination, does not lead to an immediate loss of mission functionality [39]. This shows that the system must be thoroughly tested before launch. The following parameters were chosen to be tested as they provide an overview of the efficiency, reliability, and compliance of the system with the requirements. The testing setup consists of the HAMEG HMP2030 programmable power supply [40], HM8315 RF synthesizer [41], the HMS3010 spectrum analyzer [42] and the HP 4396A network analyzer [43]. The testing setup can be seen in figure 4.1.

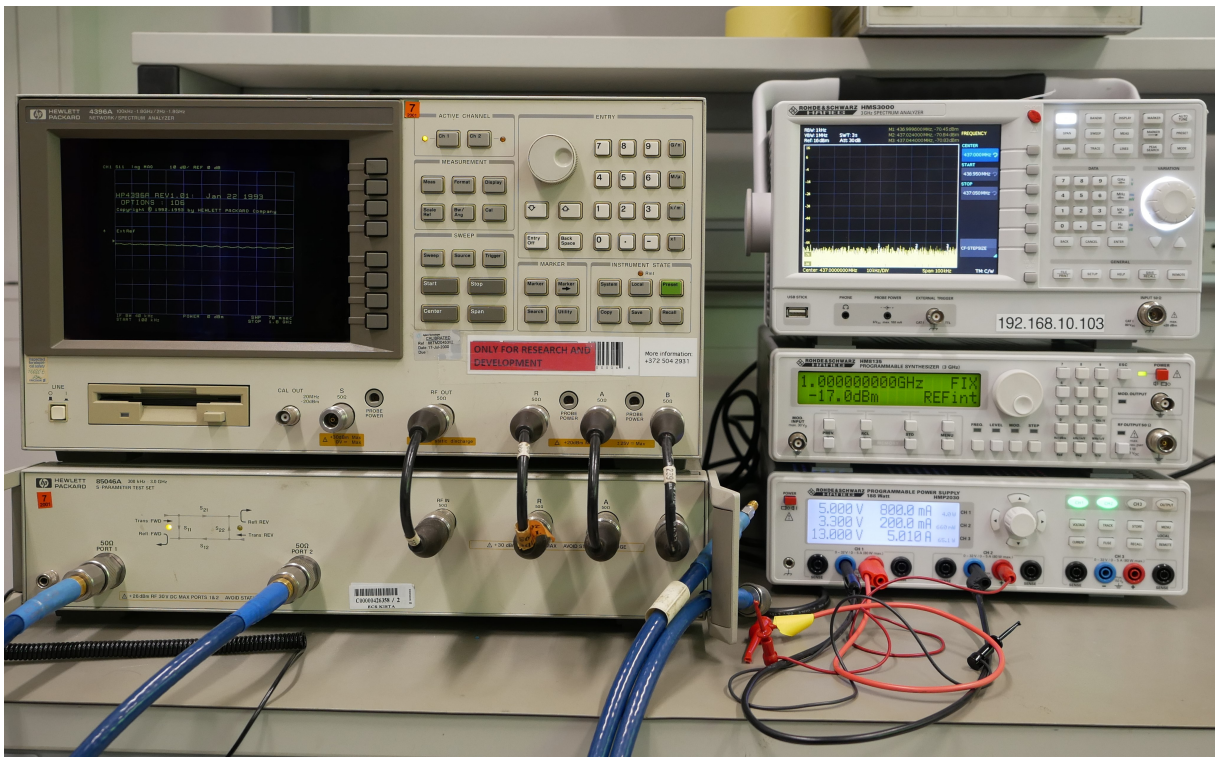

Figure 4.1. RF testing setup

4.1 Gain and Output Power

Two important characteristics of a RF PA are the output power and the gain. The gain describes the relationship between the input and output power of the system and is usually given in decibels (dB). In most cases, the gain of a PA is constant across a wide range of input power levels, but drops when the device is close to its saturation region. One of the most common metrics for characterizing a PAs maximum output power is the 1 dB compression point or P_{1dB}, which describes the operating point where the gain is exactly 1 dB lower than it would be in the linear region [44] [45].

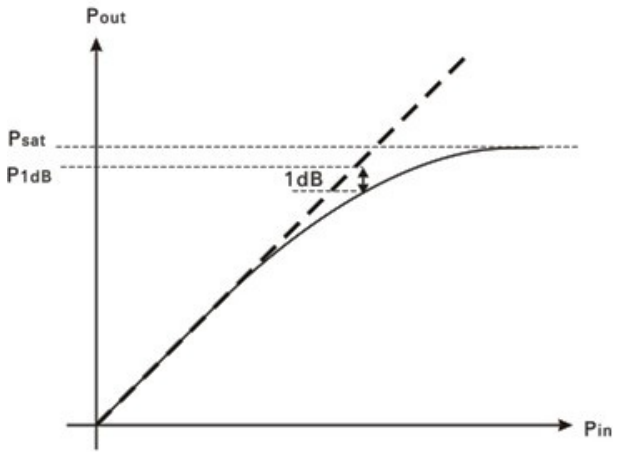

Figure 4.2. Input versus output power of a typical PA [46]

The output power, and therefore the gain, can be measured as functions of the input power. This is done by sweeping the power level of a signal generator with a ramp waveform and measuring the output of the PA using an RF spectrum analyzer. A simpler test setup involves the use of a Vector Network Analyzer (VNA), which can act as both the signal generator and the measuring device. In both cases, attenuators should be used to limit the output power and prevent damage to the measuring devices, but also to reduce mismatch uncertainty. As the attenuation factor is constant throughout the frequency spectrum, it can be added back to the results at the end. [45]

The output power of the PA can be measured by sending a continuous-wave (CW) signal from the transceiver and measuring the power at the connector placed at the output of the PA with an RF spectrum analyzer. The results can be seen in table 4.1.

Table 4.1. Measured amplifier performance at different input power levels.

Input power (dBm)	Output power (dBm)	Gain (dB)	Supply current (A)	Supply power (W)	PAE (%)
-10	28.44	38.44	0.341	1.705	40.95
-7	29.90	36.90	0.415	2.075	47.10
-5	30.35	35.35	0.458	2.290	47.33
-2	30.67	32.67	0.511	2.555	45.67
0	30.75	30.75	0.548	2.740	43.38
2	30.89	28.89	0.570	2.850	43.07
5	30.99	25.99	0.589	2.945	42.65

The measured results show that the amplifier's output power increases with input power, reaching a saturation point near 31 dBm around 0 dBm input. Beyond this level, further increases in input power produce only small increases in output power, indicating that the amplifier has reached its saturation region. At the same time, the gain decreases from 38.44 dB at –10 dBm input to 25.99 dB at 5 dBm input, indicating gain compression typical of power amplifiers as they approach their nonlinear region. The PAE exhibits a peak value of approximately

47.33% at –5 dBm input power, after which it gradually declines to 42.65% at the highest input level tested. This behavior suggests an optimal operating range near –5 dBm to –2 dBm input. The increase in supply current and power with input level corresponds with the higher output power demands but also contributes to reduced efficiency beyond the optimal point. Overall, the amplifier demonstrates its best performance in terms of efficiency and gain in the mid-input power range, while operation near saturation results in diminishing returns in output power and efficiency.

The measured output power was approximately 5 dBm lower than the values specified in the manufacturer's datasheet. To investigate the underlying cause of this discrepancy, the amplifier's scattering parameters (*S*-parameters) were measured using a vector network analyzer. The *S*-parameters can be seen in Figure 4.3.

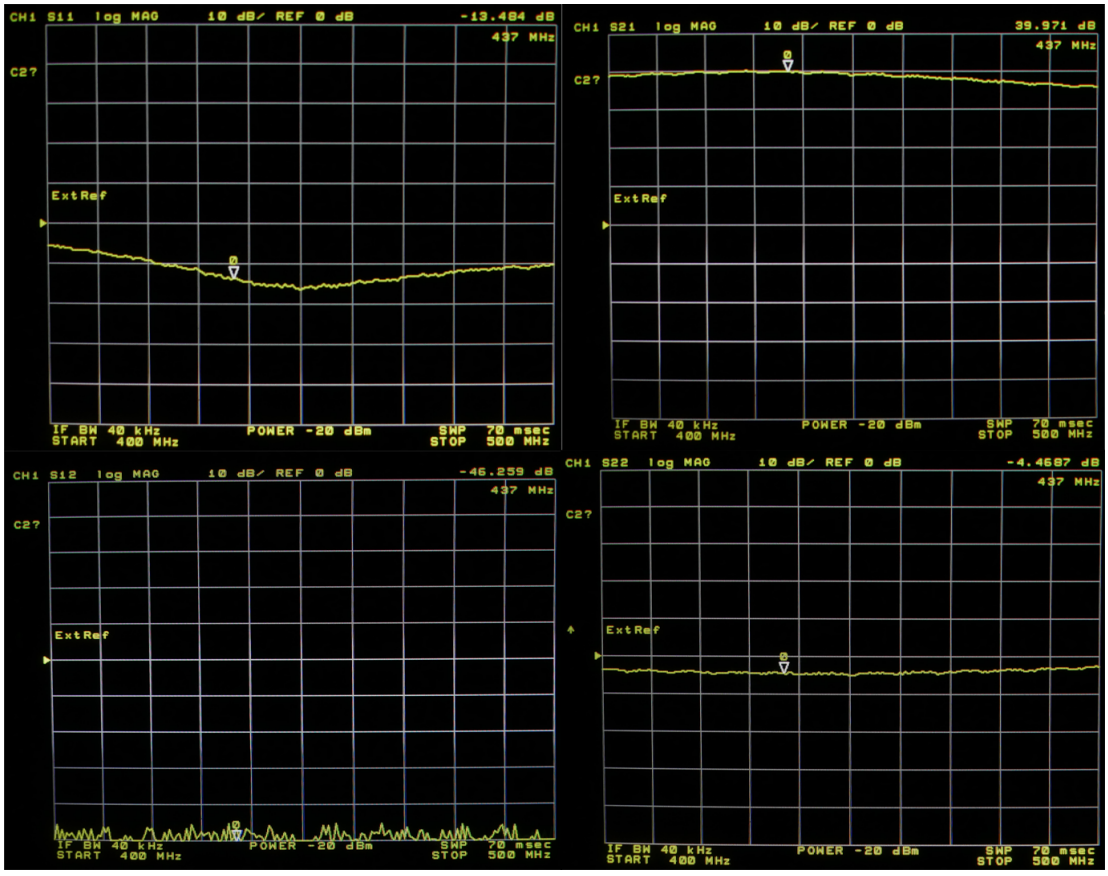

Figure 4.3. Power amplifier *S*-parameters from 400 to 500 MHz

At 437 MHz, the measured values were : $|S_{11}| = -13.48$ dB, $|S_{21}| = 39.97$ dB, $|S_{12}| = -46.26$ dB, and $|S_{22}| = -4.47$ dB.These results show a satisfactory input match (S_{11}), but a poor output match, as evidenced by the relatively high S_{22} value. Further tuning yielded a slight improvement in output matching, with $|S_{22}| = -5.12$ dB; however, this is still not a good result. A likely contributor to this mismatch is the printed circuit board (PCB) layout,

specifically the physical distance between the power amplifier (PA) output and the associated matching network.

4.2 Out-of-band and spurious emissions

Out-of-band and spurious emissions are unintended signals outside the desired bandwidth. The ITU gives out-of-band emission limits in the amateur UHF band as an emission mask, which can be seen in Figure 4.4. Assuming a 20 kHz bandwidth with a center frequency of 437 MHz, the out-of-band emission limits can be seen in the table.

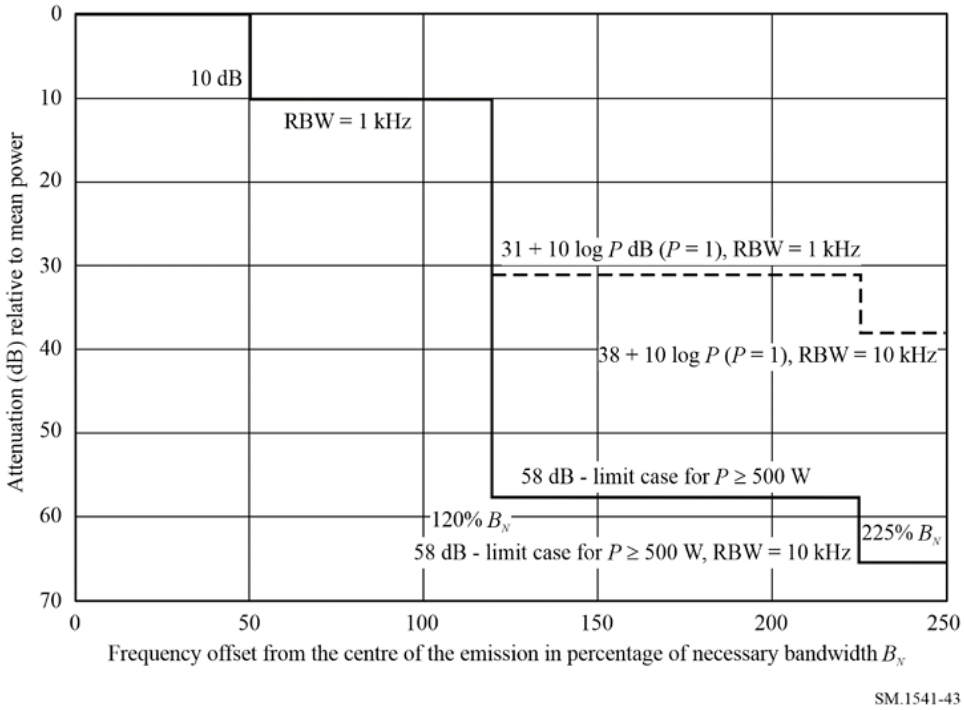

Figure 4.4. OOB emission limit from ITU-R SM.1541-7. [16]

For evaluating OOB and spurious emissions, the transmitter was connected to a spectrum analyzer through a calibrated attenuator to prevent damage to the input port. The measurement was performed with the Rohde&Schwarz HMS3000 spectrum analyzer with the following settings:

- **Center frequency:** 437 MHz
- **Span:** 1 MHz (for OOB), 100 MHz–1 GHz (for spurious)
- **Resolution bandwidth (RBW):** 1 kHz (OOB), 100 kHz (spurious)

The transmitter was configured to emit a pseudorandom PN9 sequence using GFSK modulation. For out-of-band testing, the spectrum was scanned from 437 MHz ± 500 kHz, and the emission levels were plotted against the ITU mask. For spurious emissions, the spectrum analyzer scanned from 100 kHz to 1 GHz, identifying any emissions above the 38 dBc threshold. Screenshots of the spectrum analyzer screen can be seen in figures 4.5 and 4.7.

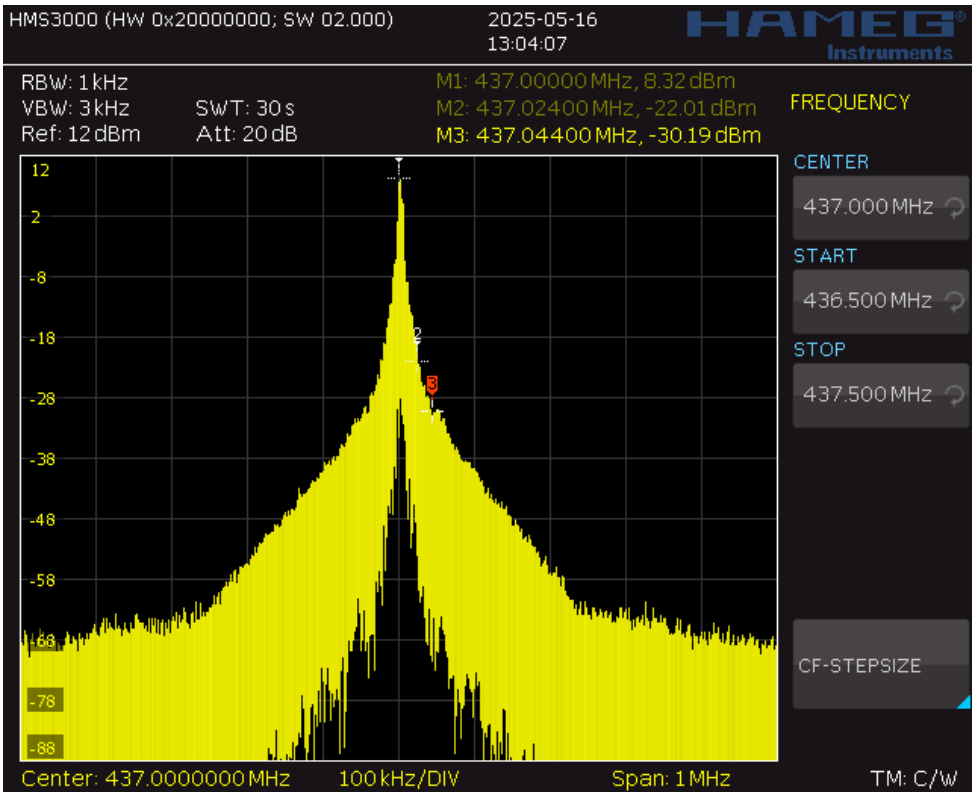

Figure 4.5. Out of band emissions using GFSK modulation

A comparison between the measured emission levels and the corresponding ITU regulatory limits reveals that the measured value at an offset of ±45 kHz slightly exceeds the specified limit. The relevant values are summarized in Table 4.2. Although filtering is already implemented at the transmitter output, this result suggests that the existing filter and output matching network should be re-evaluated and optimized to improve out-of-band suppression and guarantee adherence with the emission mask.

Table 4.2. Comparison of out-of-band emission limits and measured values

Offset Range	ITU Limit	Measured Value
±10 kHz (in-band)	–	–
±24 kHz	≤ −10 dBc	−12 dBc
±45 kHz	≤ −31 dBc	−30.3 dBc
> 45 kHz	≤ −38 dBc	−38.5 dBc

When switching from Gaussian Frequency Shift Keying (GFSK) to regular Frequency Shift Keying (FSK), a reduction in occupied bandwidth was observed. This is shown in Figure 4.6, where the measured spectrum of the FSK-modulated signal is plotted against the ITU emission mask. This outcome contradicts established theory, as the Gaussian filtering applied in GFSK is expected to reduce the bandwidth by limiting high-frequency components. Further analysis is needed to identify what may have caused this result. The FSK-modulated signal is fully compliant with the ITU out-of-band emission limits.

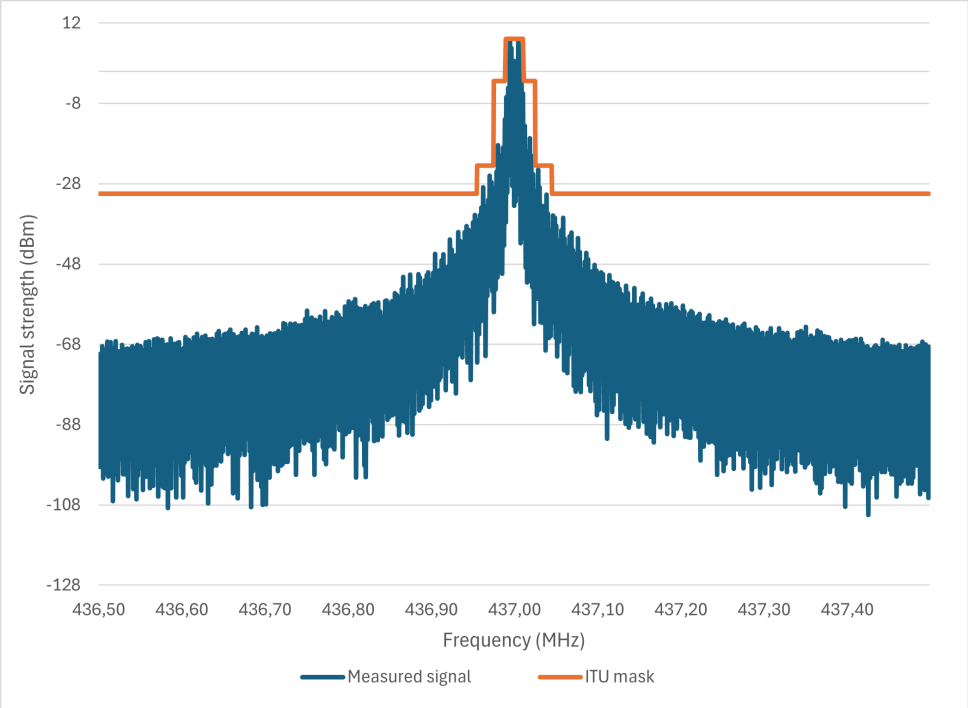

Figure 4.6. Out of band emissions using FSK modulation, plotted against ITU mask

Additionally, the only spectral component observed beyond the primary emission band was the second harmonic of the carrier, measured at $-42.6\,\mathrm{dBc}$. Although this value complies with the regulatory limit of $-38\,\mathrm{dBc}$, it is still considered relatively high and may indicate suboptimal harmonic suppression. Further research and testing are needed to find out the cause of this issue.

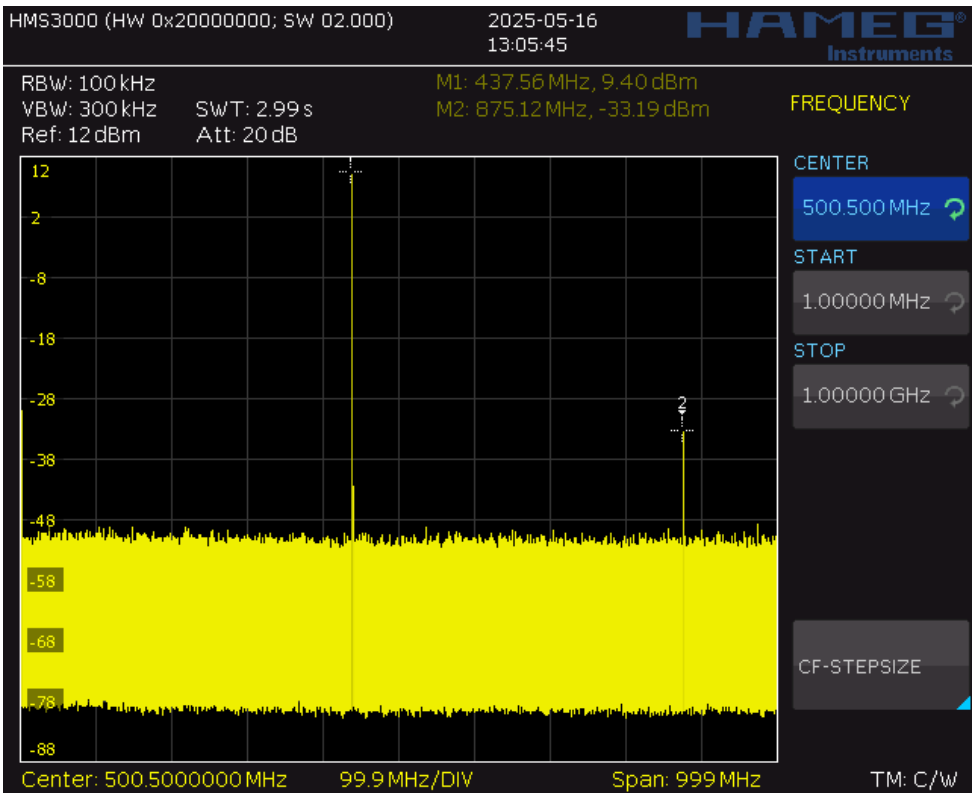

Figure 4.7. Spurious emissions

4.3 Power consumption and efficiency

The overall efficiency of the system η_{sys} is defined as the ratio of RF output power (P_{RF}) to the total DC input power consumed by the communication subsystem (P_{in}) shown in 4.1.

$$\eta_{sys} = \frac{P_{RF}}{P_{in}} \cdot 100\% \tag{4.1}$$

The COM board was powered through a calibrated digital power supply capable of accurately measuring voltage and current. The RF output was connected to an RF spectrum analyzer, and the output power was measured. Results can be seen in table 4.3.

Table 4.3. Power consumption and output power in different operating states

State	Power Consumption (mW)	Output Power
Idle	15	–
RX	53	–
TX	2380	29.4 dBm

Overall system efficiency in TX mode is

$$\eta_{sys} = \frac{10^{\frac{29.4}{10}}}{2.38} \cdot 100\% = 36.6\%. \tag{4.2}$$

The measured efficiency of 36.6% is similar to efficiency values of other communication systems of comparable missions. Still, it remains significantly lower than the efficiency specified in the datasheet of the PA. This is most likely caused by losses in the RF transmission chain. To address this, the matching at the output of the PA should be improved.

4.4 Thermal testing

Thermal testing is essential to guarantee the reliability of the communication system under operating conditions similar to the space environment. To simulate prolonged exposure to elevated thermal loads, the system was subjected to high-temperature stress testing.

For this accelerated life test, the Device Under Test (DUT) was placed inside a programmable thermal chamber, which was maintained at a constant temperature of 60°C for 6 hours. The system was set to transmit more for the duration of the whole test. This operational condition represents the worst-case scenario in terms of power dissipation and thermal stress, accelerating the aging process and showing system reliability under maximum load. Throughout the duration of the test, the DUT remained continuously active in TX mode.

After the test, output power, efficiency, and signal bandwidth were measured. No degradation or significant variation in these parameters was observed, indicating that the system maintains stable performance under high-temperature, high-duty-cycle conditions. This suggests that the design is thermally robust and suitable for operation in space conditions.

4.5 Mismatch resilience testing

To evaluate the resilience of the PA to severe impedance mismatches, a mismatch resilience test was conducted. This test simulates extreme load conditions that could occur due to antenna damage or faulty impedance matching. The objective was to assess the PA's ability to maintain safe operation and preserve its performance when subjected to high reflection coefficients.

During the test, the output of the communication system was initially left unterminated (open circuit), resulting in full signal reflection with a reflection coefficient magnitude of $|\Gamma| = 1$. After this, the output was connected to a short circuit, further stressing the PA with maximum

reverse power. These two conditions represent worst-case mismatch scenarios.

After the test, the output was connected to the spectrum analyzer, and output power, efficiency, and bandwidth were measured. No measurable change was detected, showing that the PA remained fully operational and undamaged. These results show that the system exhibits strong resilience to severe load mismatches.

4.6 Received signal strength indicator

The Received Signal Strength Indicator (RSSI) is a key metric used to evaluate the sensitivity and performance of the receiver. It provides a relative measurement of the power level received by the radio front end.

To measure RSSI, the receiver module on the COM board was connected directly to an RF synthesizer capable of generating a stable continuous-wave (CW) signal at configurable frequencies and power levels. The test signal was swept across a range of input power levels at a fixed frequency to evaluate the RSSI response.

The RSSI value was obtained by reading the internal register of the Si4668 transceiver via a serial communication interface. A formula is provided in the datasheet of the transceiver to convert the value into dBm.

The setup used for RSSI measurements is described below:

- **Signal Source:** HM8315 RF synthesizer, with output power adjustable in 1 dB steps
- **Frequency:** 437 MHz
- **Power Range:** -120 dBm to -85 dBm

The measured results can be seen in Table 4.4.

Table 4.4. Transmitted Signal vs. Received Signal Calculated from RSSI

Synthesizer Output (dBm)	Received Signal (dBm)
-	-126
-120	-126
-117	-123
-113	-119
-110	-114
-105	-110
-100	-104
-95	-98
-90	-93
-85	-89
-80	-83
-75	-78

The results in Table 4.4 show a clear and approximately linear relationship between the signal strength transmitted by the RF synthesizer and the received signal level calculated from the Si4668 RSSI register. As the input power increases, the RSSI derived signal level also increases correspondingly. With no input signal, the RSSI value is close to the noise floor calculated in the link budget.

The measured offset between transmitted and received values remains relatively consistent, averaging around -5 dB. This offset may be attributed to internal losses in the receiver front end.

5 Conclusions and future work

This thesis has presented the architecture development and experimental validation of the engineering model of the UHF communication subsystem for the Strategic Upgrades Test Satellite (SUTS), a 3-unit PocketQube satellite developed by the Estonian Student Satellite Foundation. The main goal was to design a compact, reliable, and standards-compliant communication system.

The system was implemented using the Silicon Labs Si4468 transceiver and the GRF5504 PA. The system does not have a dedicated MCU but is controlled by the satellite's CDHS. The communication subsystem was extensively analyzed and validated through a series of tests, including gain and efficiency measurements, thermal and mismatch tolerance, out-of-band and spurious emissions, and receiver sensitivity characterization.

Testing showed that the transmitter was capable of delivering a maximum output power of approximately 29.4 dBm at the antenna port. While this closely approaches the mission's 30 dBm requirement, it remains marginally below the ideal target and shows the need for improvements in the matching at the output of the PA.

The PAE of the amplifier peaked at 47.3%, with the most efficient operation observed at an input level of -5 dBm. The overall efficiency of the system, considering the power consumption of other components and signal losses in the RF front-end was 36.6%.

Emissions testing showed that while the system generally remained within spurious and out-of-band emission limits, there were minor exceedances at specific frequency offsets. To determine the cause of these results, further research and testing is needed.

No changes were observed in output power, efficiency, or bandwidth after thermal and mismatch resilience tests. This shows that the amplifier is thermally robust and capable of handling severe load mismatch.

The performance of the receiver, as characterized by RSSI measurements, showed consistent linearity across a wide range of input power levels, with an average offset of approximately -6 dB.

Before the subsystem is ready for the flight model, several areas need further work. The output matching network requires improvement to reduce the reflected power and improve overall transmission efficiency. Better filtering is also needed to bring all emissions fully within regulatory limits.

In addition to hardware improvements, proper communication software must be developed. This includes implementing protocols for packet handling, error correction, beacon transmission, and power control.

Bibliography

[1] M. N. Sweeting. „Modern Small Satellites-Changing the Economics of Space“. In: *Proceedings of the IEEE* 106.3 (2018), pp. 343–361. DOI: 10.1109/JPROC.2018.2806218.

[2] California Polytechnic State University. *CubeSat Design Specification*. Tech. rep. California Polytechnic State University, 2022. URL: https://static1.squarespace.com/static/5418c831e4b0fa4ecac1bacd/t/62193b7fc9e72e0053f00910/1645820809779/CDS+REV14_1+2022-02-09.pdf.

[3] S. Radu, M. S. Uludag, S. Speretta, J. Bouwmeester, A. Menicucci, A. Cervone, A. Dunn, T. Walkinshaw, P. L. Kaled Da Cas, and C. Cappelletti. *The PocketQube Standard Issue 1*. 2018. URL: https://static1.squarespace.com/static/53d7dcdce4b07a1cdbbc08a4/t/5b34c395352f5303fcec6f45/1530184648111/PocketQube+Standard+issue+1+-+Published.pdf.

[4] „IEEE Standard Letter Designations for Radar-Frequency Bands“. In: *IEEE Std 521-2002 (Revision of IEEE Std 521-1984)* (2003), pp. 1–10. DOI: 10.1109/IEEESTD.2003.94224.

[5] NASA. *9.0 Communications*. 2024. URL: https://www.nasa.gov/smallsat-institute/sst-soa/soa-communications/.

[6] J. Dalbins, K. Allaje, H. Ehrpais, I. Iakubivskyi, E. Ilbis, P. Janhunen, J. Kivastik, M. Merisalu, M. Noorma, M. Pajusalu, I. Sünter, A. Tamm, H. Teras, P. Toivanen, B. Segret, and A. Slavinskis. „Interplanetary Student Nanospacecraft: Development of the LEO Demonstrator ESTCube-2“. In: *Aerospace* 10.6 (2023), p. 503. DOI: 10.3390/aerospace10060 URL: https://www.mdpi.com/2226-4310/10/6/503.

[7] M.-L. Plats and S. Sarapuu. *ESTCube-2 satellite was probably destroyed on board launcher upon its re-entry to Earth*. 2023. URL: https://ut.ee/en/content/estcube-

2-satellite-was-probably-destroyed-board-launcher-upon-its-re-entry-earths.

[8] J. Dalbins, K. Allaje, I. Iakubivskyi, J. Kivastik, R. O. Komarovskis, M. Plans, I. Sünter, H. Teras, H. Ehrpais, E. Ilbis, M. Noorma, A. Slavinskis, M. Merisalu, and P. Janhunen. „ESTCube-2: The Experience of Developing a Highly Integrated CubeSat Platform“. In: *2022 IEEE Aerospace Conference (AERO)*. 2022, pp. 1–16. DOI: 10.1109/AERO53065.2022.9843521.

[9] K. Allaje. „Communications subsystem hardware and software development for the ESTCube-2 nanosatellite“. MA thesis. Tartu Ülikool, 2021.

[10] BME Műegyetemi Rádió Club. *MRC-100 Project*. Accessed: 2024-09-28. 2023. URL: https://gnd.bme.hu/mrc100/index_en.html.

[11] Y. A. I. Humad and L. Dudás. „GPS Type Tracker Based On LoRa Transmission for MRC-100 3-PocketQube Student Satellite“. In: *2022 13th International Symposium on Communication Systems, Networks and Digital Signal Processing (CSNDSP)*. 2022, pp. 98–102. DOI: 10.1109/CSNDSP54353.2022.9907953.

[12] S. Radu, S. Uludag, S. Speretta, J. Bouwmeester, E. Gill, and N. Foteinakis. „Delfi-PQ: The first pocketqube of Delft University of Technology“. In: *Proceedings of 69th International Astronautical Congress*. France: International Astronautical Federation, IAF, 2018. URL: https://www.iac2018.org/.

[13] S. Speretta, S. Uludag, V. Karunanithi, S. Radu, N. Chronas Foteinakis, J. Bouwmeester, A. Menicucci, and E. Gill. „A Multi Frequency Deployable Antenna System for Delfi-PQ“. In: *Proceedings of the International Symposium on Space Technology and Science, Fukui, Japan, June 15-21, 2019*. International Symposium on Space Technology and Science; Conference date: 15-06-2019 through 21-06-2019. 2019. URL: https://www.ists.or.jp/.

[14] C. H. Broekhuizen, S. Speretta, M. S. Uludag, M. van den Bos, J. Haenen, A. Menicucci, and E. Gill. „Miniaturized Radio Tranceiver for PocketQubes, Exceeding Performance of CubeSat Solutions“. In: *Small Satellite Conference*. Utah State University. Logan, UT, 2020. URL: https://digitalcommons.usu.edu/smallsat/2020/all2020/53/.

[15] Ergo Haavasalu. „PQ9 standardile vastav pikosatelliidi raadiosidemoodul“. 2024.

[16] „Recommendation ITU-R SM.1541-7 (09/2024) - Unwanted emissions in the out-of-band domain“. In: ().

[17] *Satellite Tracking System: Orbitron by Sebastian Stoff*. URL: https://www.stoff.pl/ (visited on 6/3/2025).

[18] Katarina Aas. „Tudengisatelliidile SUTS antenni valimine ja disainimine modelleerimistarkvaraga 4NEC2“. 2025.

[19] Simon R. Saunders and Alejandro Aragón-Zavala. *Antennas and propagation for wireless communication systems*. 2nd ed. OCLC: ocm85830855. Chichester, England ; Hoboken, NJ: J. Wiley & Sons, 2007. 524 pp. ISBN: 978-0-470-84879-1.

[20] Roger R. Bate, Donald D. Mueller, and Jerry E. White. *Fundamentals of Astrodynamics*. New York: Dover Publications, 1971. ISBN: 9780486600611.

[21] Glenn Robb. „Circularly Polarized Antennas Explained, Without The Math“. In: ().

[22] N. K. Nikolova and et al. *Lecture 7: Noise in Receiving Systems*. McMaster University, ECE 4F4 Antenna Course Lecture Notes. URL: https://www.ece.mcmaster.ca/faculty/nikolova/antenna_dload/current_lectures/L07_Noise.pdf (visited on 28/4/2025).

[23] RFM Integrated Device, Inc. *SF2446E 435 MHz SAW Filter Datasheet*. https://www.mouser.ee/datasheet/2/1100/SF2446E-3134307.pdf. Accessed: 2025-05-11. 2022.

[24] Qorvo, Inc. *RFSW1012 Broadband SPDT Switch Datasheet*. https://www.qorvo.com/products/p/RFSW1012. Accessed: 2025-05-11. 2018.

[25] Doug Layne. „Receiver Sensitivity and Equivalent Noise Bandwidth“. In: *High Frequency Electronics* (2014). Accessed: 2025-04-28. URL: https://www.highfrequencyelect
com/index.php?option=com_content&view=article&id=553:receiver-sensitivity-and-equivalent-noise-bandwidth&catid=94:2014-06-june-articles&Itemid=189.

[26] *Si4468 datasheet*. URL: https://www.silabs.com/documents/public/data-sheets/Si4468-7.pdf (visited on 14/3/2025).

[27] *GFSK — Analog Devices*. URL: https://www.analog.com/en/resources/glossary/gfsk.html (visited on 14/3/2025).

[28] *GRF5504 Data Sheet — Guerrilla RF*. URL: https://www.guerrilla-rf.com/products/DataSheet?sku=5504&file_name=GRF5504DS.pdf (visited on 22/11/2024).

[29] *AN648: Si4x6x and EZR32 High-Power PA Matching*. URL: https://www.silabs.com/documents/public/application-notes/AN648.pdf (visited on 14/3/2025).

[30] *GRF5504 Custom Tunes — Guerrilla RF*. URL: https://www.guerrilla-rf.com/products/CustomTunes?sku=5504&file_name=GRF5504%20430-435%20MHz%20Optimized%20for%20Psat%204-15-21.pdf (visited on 20/3/2025).

[31] Michael Margraf. *uSimmics – A Free and Powerful Circuit Simulator (formerly known as QucsStudio)*. URL: https://qucsstudio.de.

[32] *20.7 dB SMT Bi-Directional Coupler, 360 - 1000 MHz, 50 — BDCN-20-13+ — Mini-Circuits*. URL: https://www.minicircuits.com/WebStore/dashboard.html?model=BDCN-20-13%2B&srsltid=AfmBOopbK79qQxLsVCiyGHvgNE70O7ZRUf (visited on 23/4/2025).

[33] *AN643: Si446x/Si4362 RX LNA Matching*. URL: https://www.silabs.com/documents/public/application-notes/AN643.pdf (visited on 30/4/2025).

[34] *AD7991 Datasheet and Product Info — Analog Devices*. URL: https://www.analog.com/en/products/ad7991.html#software-resources (visited on 30/4/2025).

[35] *AD8330 Datasheet and Product Info — Analog Devices*. URL: https://www.analog.com/en/products/ad8330.html (visited on 30/4/2025).

[36] *LM26LV data sheet, product information and support — TI.com*. URL: https://www.ti.com/product/LM26LV (visited on 30/4/2025).

[37] Christopher Bowick. *RF Circuit Design*. 2nd. Norwood, MA: Artech House, 2015. ISBN: 978-0-7506-8518-4.

[38] Saturn PCB Design. *Saturn PCB Toolkit*. Accessed: 2025-04-25. 2025. URL: http://www.saturnpcb.com/pcb_toolkit.htm.

[39] M. Langer and J. Bouwmeester. „Reliability of CubeSats – Statistical Data, Developers' Beliefs and the Way Forward". In: *Proceedings of the 30th Annual AIAA/USU Conference on Small Satellites*. 2016.

[40] HAMEG Instruments GmbH. *HMP2020 / HMP2030 Programmable 2 / 3 Channel High-Performance Power Supply*. Datasheet. 2009. URL: https://www.sm5cbw.se/hameg/hmpwr/hmp2020-30-dat.pdf (visited on 17/5/2025).

[41] Rohde & Schwarz GmbH & Co. KG. *R&S® HM8135, R&S® HM8135X 3 GHz RF Synthesizer User Manual*. User Manual. 2006. URL: https://www.rohde-schwarz.com/au/manual/r-s-hm8135-r-s-hm8135x-3-ghz-rf-synthesizer-user-manual-manuals_78701-156998.html (visited on 17/5/2025).

[42] Rohde & Schwarz GmbH & Co. KG. *HMS3000/HMS3010 Spectrum Analyzer*. Datasheet. 2011. URL: https://scdn.rohde-schwarz.com/ur/pws/dl_downloads/dl_common_library/dl_brochures_and_datasheets/pdf_1/HAMEG_DB_EN_HMS3000_3010.pdf (visited on 17/5/2025).

[43] Keysight Technologies. *4396A RF Network/Spectrum Analyzer Operation Manual*. User Manual. 1993. URL: https://www.keysight.com/us/en/assets/9018-06751/user-manuals/9018-06751.pdf (visited on 17/5/2025).

[44] S. Simrock and Z. Geng. „Nonlinearity in RF Systems“. In: *Low-Level Radio Frequency Systems*. Cham: Springer International Publishing, 2022, pp. 265–286. ISBN: 978-3-030-94419-3. DOI: 10.1007/978-3-030-94419-3_7. URL: https://doi.org/10.1007/978-3-030-94419-3_7.

[45] National Instruments. *RFIC White Paper Series: Fundamentals of Power Amplifier Testing - Part 1: Basics of Power Amplifier and Front End Module Measurements*. Accessed: 2024-10-16. 2024. URL: https://www.ni.com/en/support/documentation/supplemental/16/rfic-white-paper-series--fundamentals-of-power-amplifier-testing.html.

[46] Keysight Technologies. *Input versus Output Power in a Typical PA*. Accessed: 2024-10-16. 2024. URL: https://docs.keysight.com/kkbopen/what-is-the-meaning-of-p1db-and-psat-as-stated-in-amplifier-specifications-588278275.html.

Acknowledgements

I would like to thank my supervisors, Jānis and Ivo, for their support and guidance during the writing process. I also thank Viljo Allik and the staff at the Tartu Observatory laboratories for their help and for providing the equipment needed to assemble and test the system I developed. Finally, I would like to thank my friends and family for their support and I am especially grateful to Katarina Aas for encouraging me and helping me stay motivated throughout the work on this thesis.

Appendices

A Engineering Model: Printed Circuit Board

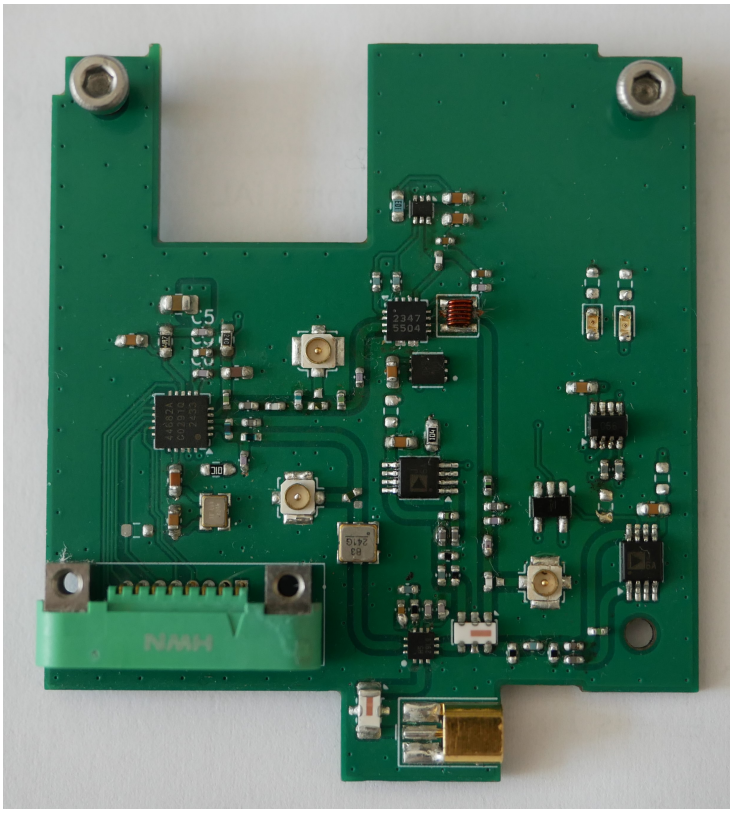

Figure A.1. Top side of the engineering model PCB. This side houses all the components.

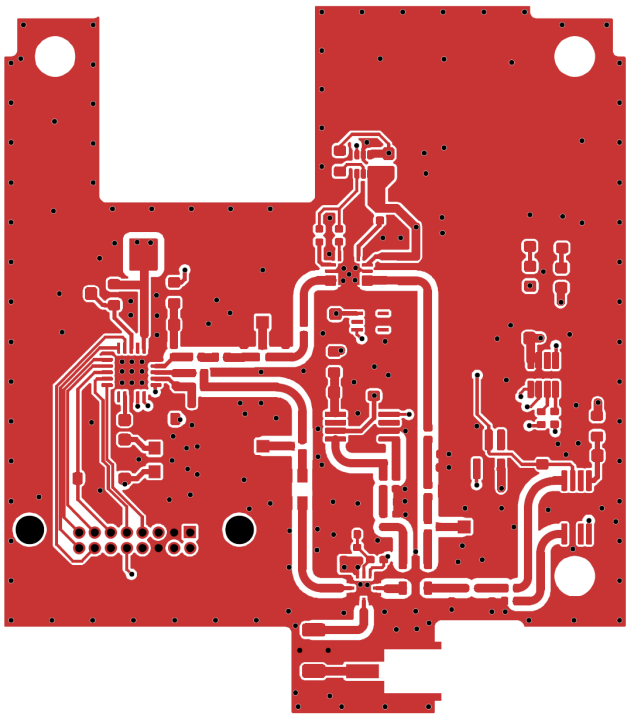

Figure A.2. The top layer houses all the components, RF traces and some signal and power traces

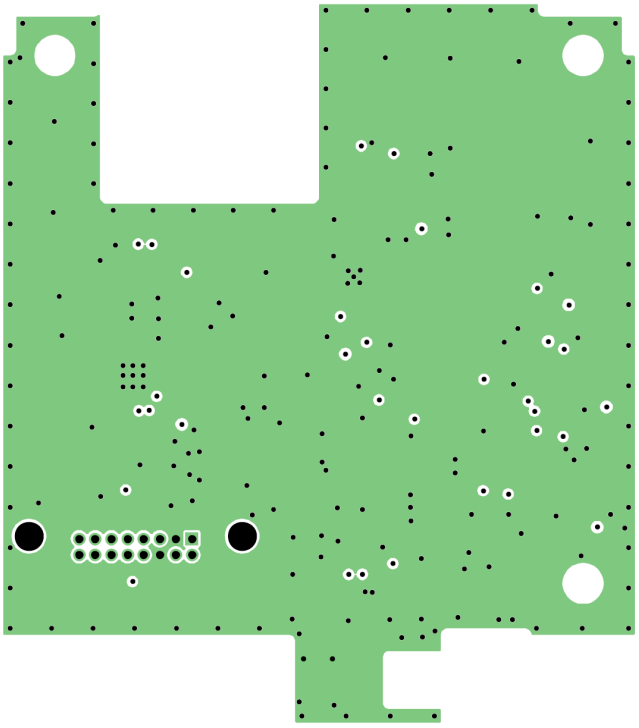

Figure A.3. The second layer from the top was allocated for ground. Together with the top layer this forms a coplanar waveguide for the RF traces

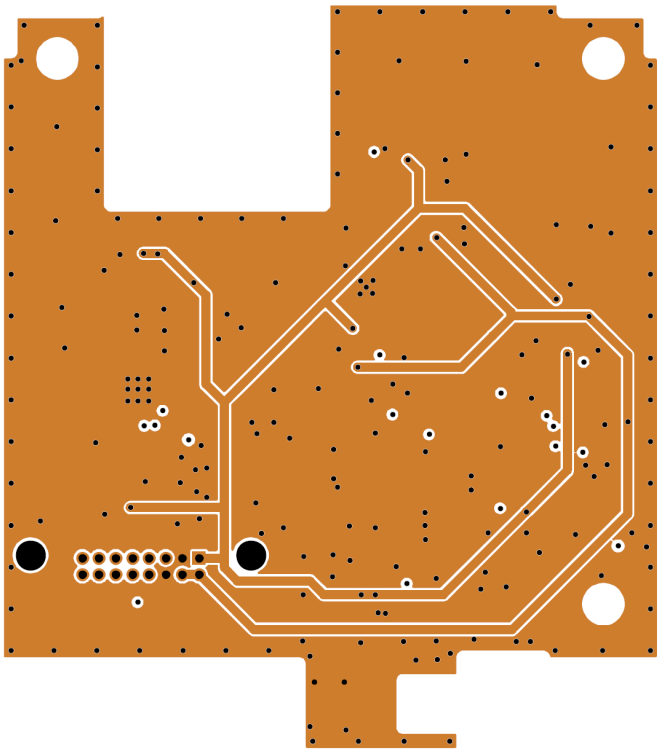

Figure A.4. The third layer from the top was allocated for distributing power to various integrated circuits.

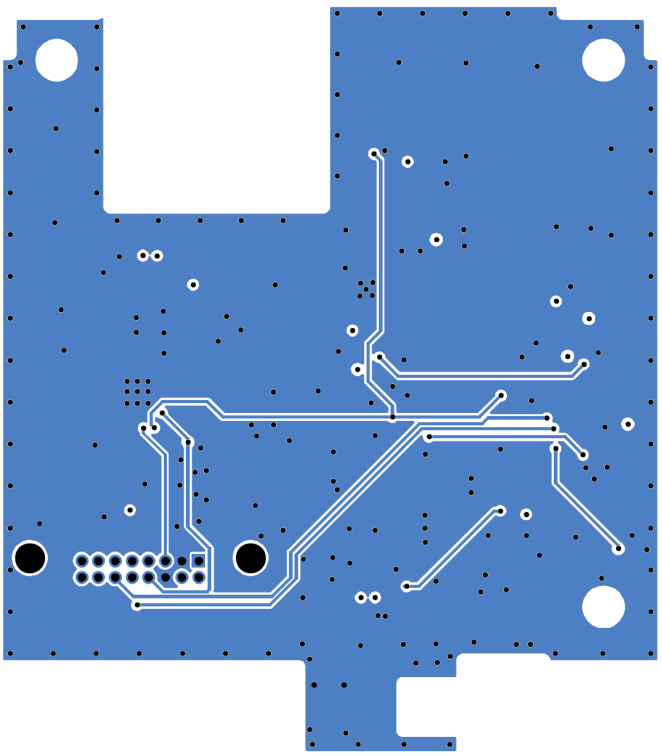

Figure A.5. The bottom layer is used for all the signal traces that couldn't be routed on the top layer

Licence

Non-exclusive licence to reproduce the thesis and make the thesis public

I, **Karl-Mattias Moor**,

1. grant the University of Tartu a free permit (non-exclusive licence) to

   reproduce, for the purpose of preservation, including for adding to the DSpace digital archives until the expiry of the term of copyright, my thesis

   "Architecture development and testing for the engineering model of SUTS satellite communication system"

   supervised by Jānis Dalbiņš and Ivo Müürsepp

2. I grant the University of Tartu a permit to make the thesis specified in point 1 available to the public via the web environment of the University of Tartu, including via the DSpace digital archives, under the Creative Commons licence CC BY NC ND 4.0, which allows, by giving appropriate credit to the author, to reproduce, distribute the work and communicate it to the public, and prohibits the creation of derivative works and any commercial use of the work until the expiry of the term of copyright.

3. I am aware of the fact that the author retains the rights specified in points 1 and 2.

4. I confirm that granting the non-exclusive licence does not infringe other persons' intellectual property rights or rights arising from the personal data protection legislation.

Karl-Mattias Moor

20.05.2025